Pergamon

Int. J. Heat Mass Transfer. Vol. 38, No. 15, pp. 2797–2807, 1995

0017-9310/95 $9.50+0.00

0017-9310(95)00027-5

Surface temperature measurement of semi-transparent material by thermocouple in real site experimental approach and simulation

A. TROMBE and J. A. MOREAU

Laboratoire d'Etudes Thermiques et Mécaniques (INSA–UPS), Complexe Scientifique de Rangueil, 31077, Toulouse cedex, France

(*Received* 12 *November* 1993 *and in final form* 28 *December* 1994)

Abstract—This study's aim is to appreciate real site surface temperature error values obtained using a thermocouple on semi-transparent materials and to determine a method of correction. Using an efficient measurement system, an experimental study was carried out under a number of climatic conditions. The results show that high values for solar radiation and wind speed have a significant influence on thermocouple measurement. The authors, therefore, decided to validate and develop a corrective model for the measurement errors of these two parameters. The conclusion also provides data on the model's relative drawbacks and current limitations.

1. INTRODUCTION

Glass is now widely used in building construction and can have considerable influence on building consumption and on the thermal comfort conditions of dwellings. It is therefore of prime importance to determine surface temperatures accurately.

Forms of interference in the use of contact thermometric sensors have been studied for a number of years now. But, obviously, it is difficult to consider the phenomenon generally as experimental conditions, the facilities used and expected results can vary considerably from one case to another. Bibliographic research has allowed us to identify a number of articles on work carried out in relation to temperature measurement and related errors. A non-exhaustive list of such work is provided by Kinzie [1].

Interesting experimental and theoretical work on surface temperature measurement through contact has been carried out by Bardon [2] and Bardon and Cassagne [3] on opaque materials. More recently, numerous authors developed such work, but on semi-transparent materials. As far as artificial sites are concerned, we can cite work by Cerruti [4] and Werling [5], and, for real sites, work by Grenier [6] and Moreau [7] can be mentioned. The authors applied the general thermocouple measurement technique as such devices are cheaper than platinium resistances, for example, and any reasonably equipped laboratory can produce them.

Note that such recent work has been carried out as part of a concerted research action of CNRS–PIRSEM of France and with the collaboration of several other laboratories mentioned below.†

Our laboratory's task was to study the influence of real meteorological conditions on surface temperature measurement error.

2. DESCRIPTION OF EXPERIMENTATION

We used a remarkable experimental system to evaluate measurement error. This comprised a semi-transparent plastic material known as polymethyl methacrylate (PMMA) with a thickness of 8.0 mm and in which three 0.2 mm diameter thermocouples are inserted (Figs. 1 and 2). This experimental system is justified by the fact that thermocouples cannot be inserted inside ordinary glass. We therefore chose a similar material whose general properties are close to

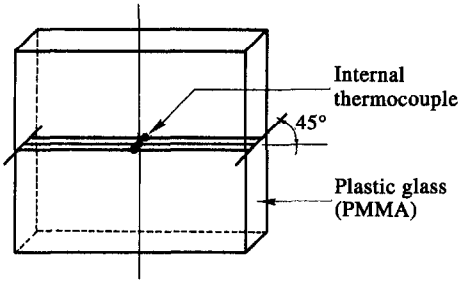

Fig. 1. Thermocouple insertion inside semi-transparent material made of plastic (PMMA).

† Laboratoire de Thermocinetique (URA CNRS 869) de l'Université de Nantes; Laboratoire d'Equipements Thermique de l'habitat de L'INSA de Lyon; Laboratoire de Fluides-Automatiques-Systemes Thermiques (URA CNRS 871) d'Orsay; Laboratoire de Mécanique des Fluides et de Thermique de l'INSA de Lyon.

NOMENCLATURE

C_f local rub coefficient
C_p constant pressure thermal capacity [J kg^{-1} K^{-1}]
D_b, D_c bar equivalent diameter and sensor head diameter [m]
D_{cc} contact diameter of sensor ($D_{cc} = 2R_{cc}$) [m]
E_o vertical solar radiation [W m^{-2}]
E_p thickness of fixation and/or protection processes [m]
F_b, F_c thermal balance of equivalent bar and sensor head [W]
H_{cb}, H_{cc} convective superficial heat exchange coefficients [W m^{-2} K^{-1}]
H_{rb}, H_{rc} radiative superficial heat exchange coefficients [W m^{-2} K^{-1}]
H_{gb}, H_{gc} overall superficial heat exchange coefficients [W m^{-2} K^{-1}] ($H_{gb} = H_{cb} + H_{rb}$ and $H_{gb} = H_{cc} + H_{rc}$)
K extinction coefficient [m^{-1}]
L_b length of calculated thermal balance [m]
Pr Prandtl number
r normal incident reflexion coefficient
R overall thermal resistance ($R = R_m + R_{ct} + R_{i1}$) [K W^{-1}]
R_{ct} contact thermal resistance [K W^{-1}]
R_{eb}, R_{ec} overall thermal resistance of superficial heat exchanges [K W^{-1}]
R_{i1}, R_{i2} thermal resistances of fixation and/or protection system processes [K W^{-1}]
R_m macroconstriction thermal resistance [K W^{-1}]
R_p calculated radius surface of fixation paste [m]
S_{ab}, S_{ac} absorption surfaces [m^2]
S_{eb}, S_{ec} exchange surfaces [m^2]
T_a ambient temperature close to equivalent bar [°C]
T_{af} external temperature of air [°C]
T_b, T_c equivalent bar and sensor head temperatures [°C]
T_{eb}, T_{ec} equivalent bar and sensor head temperatures [°C]
T_m surface temperature measured by the sensor [°C]
T_{ms} sensor head temperature between glass and fixation and/or protection after processes [°C]
T_s surface temperature calculated using a model of semi-transparent material [°C]
T_v real surface temperature [°C]
V_∞ mean wind speed [m s^{-1}].

Greek symbols

α_b, α_c short wavelength absorption coefficient
δ distance between connection wires (equivalent bar) and semi-transparent material [m]
λ_b thermal conductivity [W m^{-1} K^{-1}]
λ_{mst} semi-transparent material's thermal conductivity [W m^{-1} K^{-1}]
λ_p thermal conductivity of fixation and/or protection processes [W m^{-1} K^{-1}]
ρ voluminal mass [kg m^{-3}]
σ Stefan–Boltzmann constant [W m^{-2} K^{-4}]
Φ outlet thermal flux of semi-transparent material [W]
Φ_b, Φ_c equivalent bar and sensor head thermal fluxes [W]
Φ_{sb}, Φ_{sc} solar radiation absorbed by equivalent bar and sensor head [W].

Subscripts

b connection wires (equivalent bar)
c sensitive part of sensor (thermocouple head).

those for ordinary glass. The main difference concerns the conductivity coefficient, which is equal to 0.2 W m^{-1} K^{-1} (Table 1).

This semi-transparent reference material was manufactured by the Thermokinetic Laboratory of the University of Nantes.

Using these thermocouples we are able to define an internal temperature field allowing us to determine the real surface temperature 'T_v' of the semi-transparent material by extrapolation. However, as solar radiation passes through the semi-transparent material (PMMA), internal thermocouples will absorb such radiative flux and their thermal behaviour will become equivalent to that for an internal heat source. Therefore, to calculate the real surface temperature 'T_v' these measurements have to be corrected. Several models were developed. Using the Cerruti model [4], we can quantify radiative heat transfer inside a semi-transparent material and, consequently, the error due to solar radation absorption by internal thermocouples. Table 2 gives the error for an internal thermocouple receiving the highest level of solar radiation (near the outside surface of the semi-transparent material).

Work carried out by Cerruti [4] and Werling [5] demonstrated that the specific emissivity of the semi-transparent material is negligible and that radiative heat transfer inside the semi-transparent material is

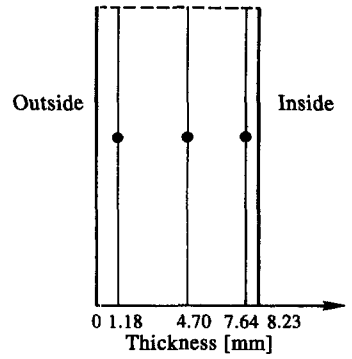

Fig. 2. Thermocouple insertion inside plastic semi-transparent material (PMMA).

only taken into account for absorption and diffusion of solar radiation. Consequently, we chose a model whose absorption satisfies Beer's law in order to determine the real surface temperature 'T_v':

$$T_{(x)} = A \times x + B + \frac{r-1}{\lambda_{mst} \times K} \times E_0 \times \exp(Kx) \quad (1)$$

where A and B represent integration constants obtained from experimental data and λ_{mst} is the conductivity coefficient value of the semi-transparent material, kept constant for

$$T_{(x=0)} = B + \frac{r-1}{\lambda_{mst} \times K} \times E_0 \quad (2)$$

and

$$T_{(x=E)} = A \times e + B + \frac{r-1}{\lambda_{mst} \times K} \times E_0 \times \exp(-Kxe). \quad (3)$$

With these corrections the error in the real surface temperature measurement is finally brought back down to ± 0.07°C.

For direct surface measurement of semi-transparent materials we used 2 mm diameter thermocouples whose initial calibration leads to an error measurement of ± 0.2°C.

They are fixed following a technique defined by Werling [5]. The head of the sensor is stuck with a conductive paste ($\lambda_p = 2.5$ W m^{-1} K^{-1}) to the inner and outer surface of the semi-transparent material. Wires of equivalent bar are stretched along the semi-transparent material's surface so as to follow, where possible, an isothermal line.

Finally, a south oriented cell, Fig. 3, equipped with a weather station, provided support for the entire experimental system.

Table 2. Influence of incident solar radiation upon temperature pertubation inside a semi-transparent material (PMMA)

E_0 [W m^{-2}]	200	400	600	800
T_c [°C]	0.05	0.1	0.15	0.2

3. EXPERIMENTAL RESULTS

The results correspond to significant solar radiation and wind speed climatic sequences that we selected from experimental data.

3.1. *Study of solar radiation's influence on measurement*

This study is presented at different times and for various solar radiation values and flow wind speed values ($V_\infty < 1$ m s^{-1}) (Figs. 4–6).

These curves show that internal temperature measurements (*) of the plastic semi-transparent material are aligned when there is no solar radiation (during the night) or when solar radiation values are lower than 150 W m^{-2} (Figs. 4 and 5). However, for higher solar radiation values, Fig. 6, it can be seen that internal temperatures are not aligned. This confirms that the semi-transparent material absorbs solar radiation.

On the other hand, we can see that direct surface temperature measurements (*) of all these curves do not have the same value as for measurements extrapolated (●) from the internal temperature field. These differences represent surface temperature measurement errors for a semi-transparent material which will be investigated in the next section.

3.2. *Study of wind speed's influence on measurement*

Figure 7 shows the influence of wind speed on direct surface measurement. When the wind speed increases, the positive difference $T_m - T_v$ decreases, and, finally, for high wind speeds, becomes negative on the outer semi-transparent material surface.

Table 1. General characteristics of semi-transparent materials

Type of material	Ordinary glass	Plastic (PMMA)
Thickness [mm]	8	8
Conductivity coefficient [W m^{-1} K^{-1}]	1.15	0.2
Extinction coefficient [m^{-1}]	15	20
Total emissivity	0.95	0.95
Solar absorption coefficient	0.06†	0.15†

†Normal incidence.

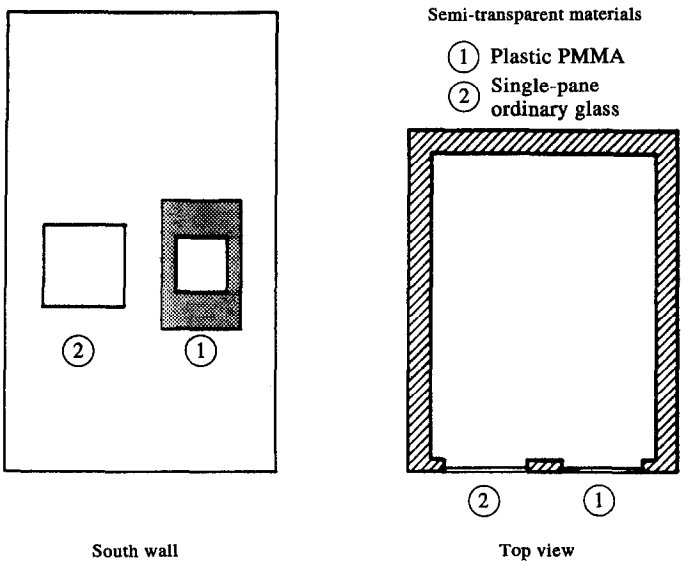

Fig. 3. Experimental cell: semi-transparent material positions.

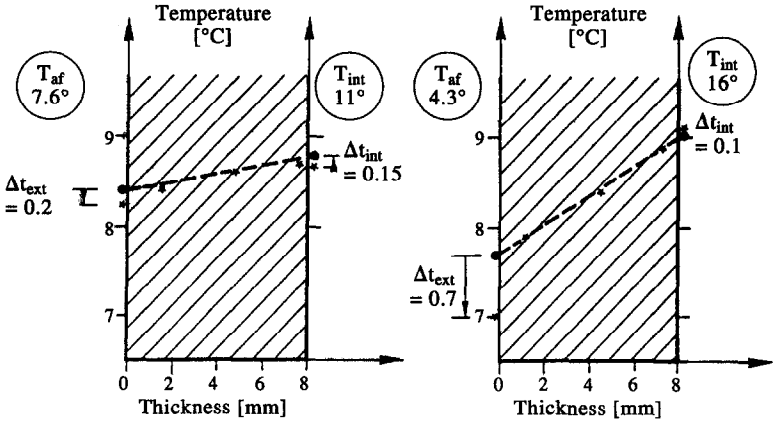

Fig. 4. Internal and surface temperatures measured in semi-transparent material (PMMA) at different times during the night and for wind speed < 1 m s^{-1}.

This observation provides confirmation that convective heat exchanges can have a significant influence on the surface measurement error.

4. MODEL DESCRIPTION

4.1. *Aim of model*

Systematic reproduction of recorded discrepancies for different solar radiation values and wind speed values has led us to develop a corrective model for surface temperature measurement of semi-transparent materials. This model's aim is to reduce experimental differences between the measured surface temperature and the equivalent true value obtained through extrapolation for all cases (Fig. 8).

4.2. *Assumptions*

Our theoretical model must take the respective influences of wind and solar radiation into account, but must also integrate other thermal phenomena depending on measurement techniques. If we consider a temperature sensor such as a thermocouple applied to a semi-transparent material, it can be represented, Fig. 9, by a physical diagram. This approach has led us to make the following prior assumptions:

(1) thermocouple fixation and/or protection processes are represented by two thermal resistances, R_{i1} and R_{i2};

(2) contact imperfections between the thermocouple and the semi-transparent material are taken into account by a contact resistance denoted R_{ct};

(3) line flux convergence at the measurement location is taken into account by a macroconstriction resistance R_m;

(4) thermocouple wires are assumed to be the equivalent bar with a given diameter and parallel to the semi-transparent measurement surface;

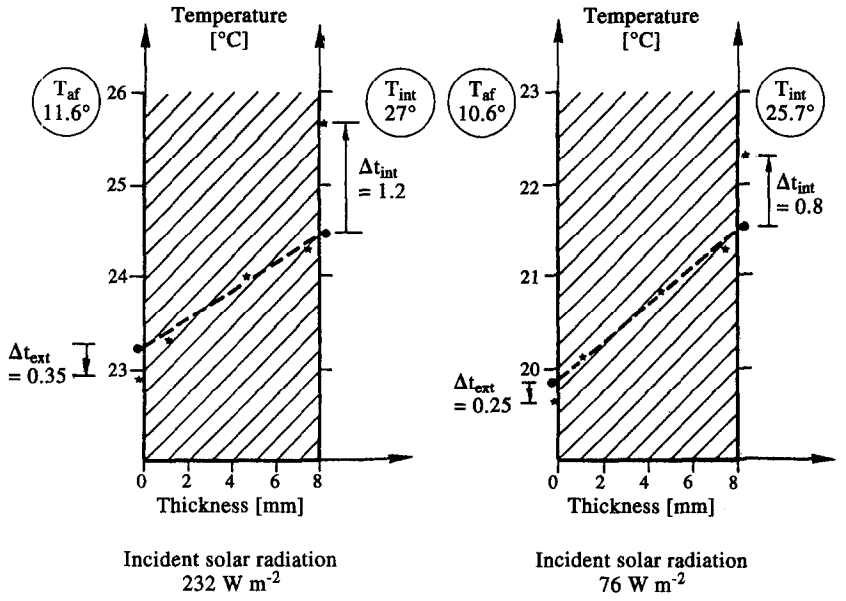

Fig. 5. Internal and surface temperatures measured in semi-transparent material (PMMA) at different times with no wind and for low incident solar radiation (<250 W m^{-2}).

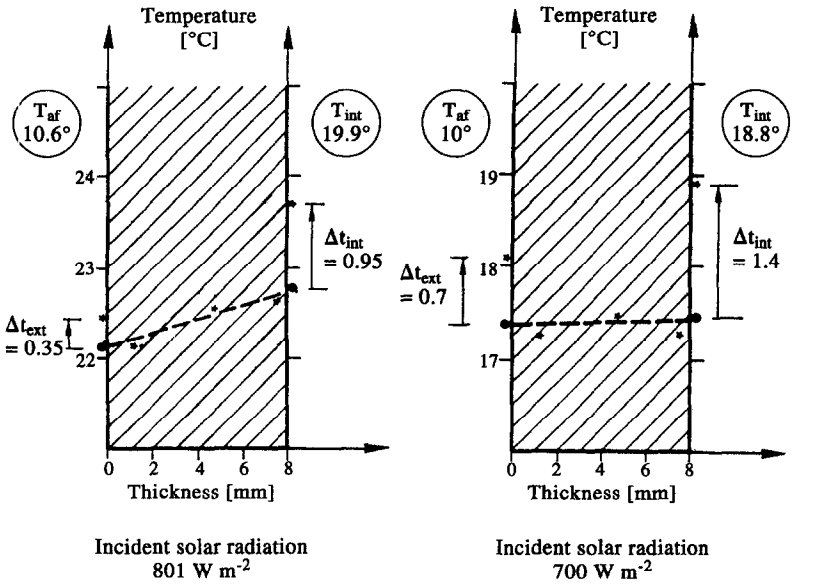

Fig. 6. Internal and surface temperatures measured in plastic material (PMMA) at different times and for high incident solar radiation (>700 W m^{-2}).

(5) finally, superficial exchanges occurring extremely close to the sensitive part of the sensor (thermocouple head) and the equivalent bar (connection wires) are represented by two overall thermal resistances, R_{ec} and R_{eb}.

4.3. *Set of equations*

The analogical diagram shown in Fig. 10 allows us to write a set of equations whose different terms are defined in the nomenclature above:

$$T_s - T_p = R_m \times \Phi \quad (4)$$

$$T_p - T_m = (R_{ct} + R_{i1}) \times \Phi \quad (5)$$

$$T_m - T_{eb} = R_{eb} \times \Phi_b \quad (6)$$

$$T_m - T_{ms} = R_{i2} \times \Phi_c \quad (7)$$

$$T_{ms} - T_{ec} = R_{ec} \times \Phi_c \quad (8)$$

$$\Phi = \Phi_b + \Phi_c \quad (9)$$

where equation (9) satisfies the first energy con-

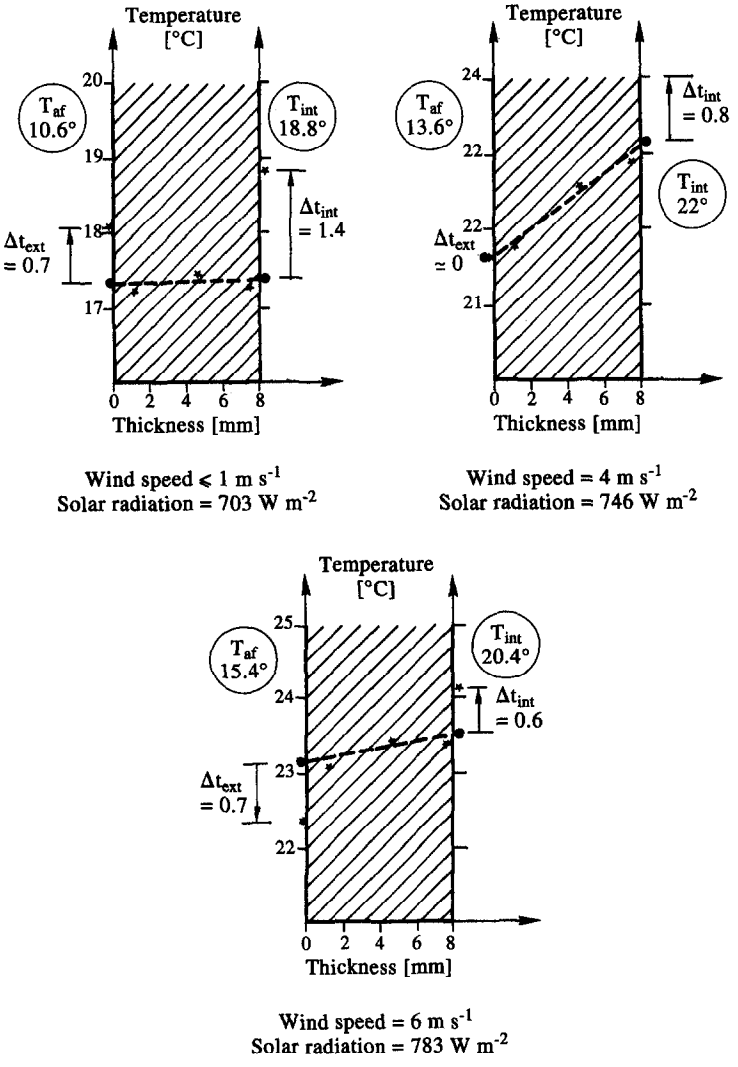

Fig. 7. Internal and surface temperatures measured in plastic material (PMMA) at different times for high incident solar radiation values (>700 W m^{-2}) and for varying wind speed values.

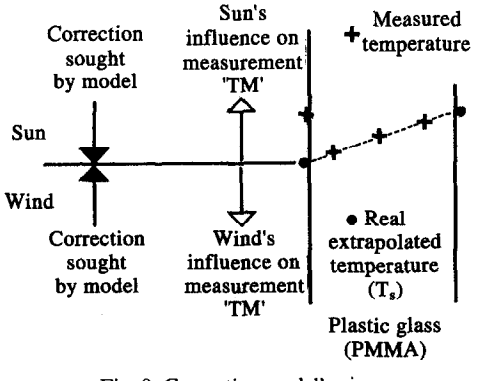

Fig. 8. Corrective model's aim.

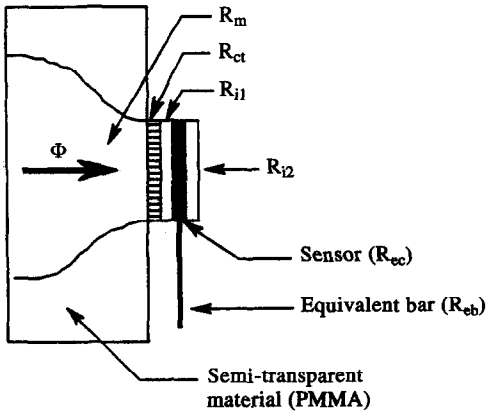

Fig. 9. Physical diagram of semi-transparent material and applied surface thermocouple.

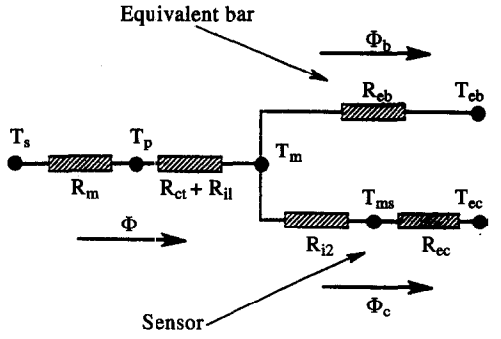

Fig. 10. Analogical diagram.

servation principle, and the flux Φ represents the sum of evacuated fluxes along connection wires and the sensor's sensitive part.

If we add equations (4) and (5) we obtain the following relation:

$$T_s - T_m = (R_m + R_{ct} + R_{il}) \times \Phi = R \times \Phi \quad (10)$$

with:

$$R = R_m + R_{ct} + R_{il}. \quad (11)$$

Equation (5) gives:

$$\Phi_b = \frac{T_m - T_{eb}}{R_{eb}}. \quad (12)$$

If we add equations (7) and (8) we obtain the following relation:

$$T_m - T_{ec} = (R_{ec} + R_{i2}) \times \Phi_c. \quad (13)$$

If we take into account equation (9) we can write:

$$\frac{T_s - T_m}{R} = \frac{T_m - T_{eb}}{R_{eb}} + \frac{T_m - T_{ec}}{R_{ec} + R_{i2}}. \quad (14)$$

This last equation allows the value of 'T_s' representing the real surface temperature calculated by our model in relation to the different thermal resistances and equivalent temperatures to be determined:

$$T_s = T_m \times \left\{1 + \frac{R}{R_{eb}} + \frac{R}{R_{ec} + R_{i2}}\right\} - R \times \left\{\frac{T_{eb}}{R_{eb}} + \frac{T_{ec}}{R_{ec} + R_{i2}}\right\}. \quad (15)$$

As we only know the value of 'T_m', we now need to calculate 'T_s' in order to evaluate all parameters for the second member of equation (15).

4.4. *Evaluation of main terms*

4.4.1. *Calculation of equivalent temperature* T_{ec}. This equivalent temperature is associated with the sensor's sensitive part (thermocouple head). It was calculated by writing a thermal balance F_c for the surface S_{ec} sensor's sensitive part:

$$F_c = H_{rc} \times S_{ec}(T_{ms} - T_r) + H_{cc} \times S_{ec}(T_{ms} - T_{af}) - \Phi_{sc} \quad (16)$$

where Φ_{sc} represents solar radiation absorbed by the sensor head:

$$\Phi_{sc} = \alpha_c \times E_0 \times S_{ac} = \alpha_c \times E_0 \times \frac{\Pi \times D_c^2}{4}. \quad (17)$$

F_c can take a more simple form, as expressed in terms of the following parameters:

T_{ec} being the equivalent temperature sought for;

H_{gc} being an overall superficial exchange coefficient with: $H_{gc} = H_{cc} + H_{rc}$

$$F_c = H_{gc} \times S_{ec}(T_{ms} - T_{ec}). \quad (18)$$

If we assume equations (17) and (18) to be equal, we can write:

$$T_{ec} = \frac{H_{cc} \times T_{af} + H_{rc} \times T_r \times \left(\alpha_c \times \frac{E_0}{2}\right)}{H_{gc}}. \quad (19)$$

4.4.2. *Calculation of equivalent temperature* T_{eb}. Applying the same reasoning, we can write a thermal balance for a length L_b of the equivalent bar:

$$F_b = H_{rb} \times \frac{S_{eb}}{2}(T_b - T_s) + H_{rb} \times \frac{S_{eb}}{2}(T_b - T_r) + H_{cb} \times S_{eb}(T_b - T_a) - \Phi_{sb} \quad (20)$$

with:

$$S_{eb} = \Pi \times D_b \times L_b \quad (21)$$

$$\Phi_{sb} = \alpha_b \times E_0 \times S_{ab} = \alpha_b \times E_0 \times D_b \times L_b. \quad (22)$$

Two other calculations were needed. They concern, respectively, the ambient temperature T_a and the convective superficial exchange coefficient H_{ca} close to the equivalent bar.

These two terms are given by the following equations:

$$T_a = T_s - \frac{H_{ca} \times \delta}{\lambda}(T_s - T_{af}) \quad (23)$$

$$H_{ca} = 0.5 \times \rho \times V_\infty \times C_p \times C_f \times Pr^{-2/3}. \quad (24)$$

The equivalent bar temperature T_{eb} is written as an expression of F_b:

$$F_b = H_{gb} \times S_{eb}(T_b - T_{eb}). \quad (25)$$

Equality between equations (20) and (25) and using relations (22) and (23) allows the final equation for T_{eb} to be obtained:

$$T_{eb} = \frac{1}{H_{gb}}\left[\frac{H_{rb}}{2}(T_s + T_r) + H_{cb} \times T_s + \frac{\alpha_b \times E_0}{\Pi} - \frac{H_{cb} \times H_{ca} \times \delta}{\lambda}(T_s - T_{af})\right]. \quad (26)$$

4.4.3. *Thermal resistance determinations*

4.4.3.1. *Macroconstriction resistance.* As the contact zone between the sensor head of the thermocouple and the semi-transparent material can satisfy the condition determined by the work of Yovanovitch *et al.* [8] and

Cassagne [9], we considered the macroconstriction resistance to be independent of boundary conditions on the opposite face.

Thus, the macroconstriction resistance representing line flux convergence towards the measurement zone is given by the following equation [10]:

$$R_m = \frac{1}{2 \times D_{cc} \times \lambda_{mst}}. \quad (27)$$

For the purpose of our study, the contact diameter D_{cc} was evaluated as 0.4 mm.

4.4.3.2. *Thermal contact resistance.* The contact resistance value is difficult to determine, as contact between two solids is only effective through a small surface area, in the middle of which is situated the interface material (conductive paste). Several methods requiring an accurate description of the cross-section are governed by perfectly well known geometrical rules [11, 12]. As it is not our case we finally chose to assimilate the contact resistance R_{ct} with the thermal resistance of the conductive paste which is used to fix the temperature sensor's head.

R_{ct} can therefore be expressed by the following relation:

$$R_{ct} = \frac{E_p}{\lambda_p \times \Pi \times R_{cc}^2}. \quad (28)$$

4.4.3.3. R_{i1} *fixation and* R_{i2} *thermal resistance protection.* These values represent the conductive paste's influence on measurement. Our experimental observations led us to adopt a conventional formulation:

$$R_{ii} = \frac{E_p}{\lambda_p \times \Pi \times R_p^2}. \quad (29)$$

4.4.3.4. *Thermal resistance* R_{ec}. This represents the overall thermal heat exchanges on the sensor's sensitive part:

$$R_{ec} = \frac{1}{H_{gc} \times S_{ec}} \quad (30)$$

with

$$H_{gc} = H_{cc} + H_{rc} \quad (31)$$

where H_{gc} represents overall superficial exchanges by convection (H_{cc}) and radiation (H_{rr}), and S_{ec} is equal to the sensor exchange surface (thermocouple head) for fixation and/or protection processes. For our calculations we assumed that it was a half-sphere:

$$S_{ec} = \frac{1}{2}\left\{4 \times \Pi \times \left[\frac{D_c}{2}\right]^2\right\}. \quad (32)$$

4.4.3.5. *Thermal resistance* R_{eb}. This thermal resistance represents overall superficial exchanges close to the equivalent bar. As this can be assumed to correspond to a fin effect, the superficial thermal resistance was determined by the following relation:

$$R_{eb} = \frac{2}{\Pi \times D_b \sqrt{(H_{gb} \times \lambda_b \times D_b)}} \quad (33)$$

with

$$H_{gb} = H_{cb} + H_{rb}. \quad (34)$$

Note that some terms appearing in the equivalent temperature determination have not been defined, but, as they are expressions or classical assumptions about convective or radiative heat exchange coefficients, they are provided in the Appendix.

5. VALIDATION OF MODEL ON SEMI-TRANSPARENT MATERIAL (PMMA)

Validation of the corrective model was carried out using real site measurements obtained from a plastic semi-transparent material (PMMA) and covering several climatic sequences. Only two of these were selected to show our model's advantage when strong climatic conditions relating wind speed and solar radiation occur.

The first set of measurements corresponds to low wind speed values ($V_\infty < 1.6$ m s^{-1}) and high solar radiation values ($E_0 > 700$ W m^{-2}).

The second set of measurements presents irregular and low solar radiation values and higher wind speed values ($2.1 < V_\infty < 4.2$ m s^{-1}).

For each of these climatic sequences a table illustrates successive values for:

(1) surface temperature measurement T_m;
(2) wind velocity V_∞;
(3) outside ambient temperature T_{af};
(4) vertical incident overall solar radiation on semi-transparent material E_0;
(5) real surface temperature T_v;
(6) corrected surface temperature T_s and
(7) temperature difference $T_s - T_v$, denoted ΔT.

Further, if we consider a real case contact resistance value R_{ct}, and fixation and/or protection resistances values, R_{ii} will not be equal to zero. These values were determined using equations (28) and (29), respectively.

To evaluate R_{ct}, equation (28) was used, assuming its value to be equal to the fixation conductive paste's thermal resistance:

(a) conductive paste thickness $E_p = 0.5$ mm;
(b) paste conductivity coefficient $\lambda_p = 2.5$ W m^{-1} K^{-1} and
(c) contact radius of the sensitive part of the thermocouple $R_{cc} = 0.2$ mm.

Numerical application gives $R_{ct} = 1600$°C W^{-1}.

To evaluate R_{ii}, equation (29) was used. Experience shows that the fixation resistance R_{i1} is included implicitly in the value for R_{ct}. It is therefore sufficient to determine the value of R_{i2}:

(a) thickness of conductive paste for protection $E_p = 0.5$ mm;
(b) paste conductivity coefficient $\lambda_p = 2.5$ W m^{-1} K^{-1} and
(c) sensor contact radius R_p ($D_c/2$) = 0.2 mm.

Table 3.†

T_m [°C]	V [m s^{-1}]	T_{af} [°C]	E_0 [W m^{-2}]	T_v [°C]	T_s [°C]	ΔT [°C]
24.9	1.1	15.4	729	24.5	24.2	−0.3
26.5	1	16.1	739	26	25.8	−0.2
27	1.1	15.7	745	26.8	26.7	−0.2
17.3	1.4	8.6	738	17	16.9	−0.1
18.2	1.2	9	759	17.9	17.7	−0.2
19.5	1.1	9.6	775	18.9	18.8	−0.1
19.6	1.6	10	781	19.5	19.6	+0.1
20.7	1.1	10.7	783	20.1	20	−0.1
21.7	1.1	10.8	775	21.3	21.2	−0.1
22.8	1.1	11.1	748	22.7	22.6	−0.1
23.1	0.9	11.1	724	22.7	22.5	−0.2
22.7	1.2	11.4	702	22.9	22.7	−0.2

† Thermal resistances (R_{ct} = 1600°C W^{-1} ; R_{i2} = 80°C W^{-1}). Low wind speed values (V_∞ < 1.6 m s^{-1}). High solar radiation values (E_0 > 700 W m^{-2}).

Table 4.†

T_m [°C]	V [m s^{-1}]	T_{af} [°C]	E_0 [W m^{-2}]	T_v [°C]	T_s [°C]	ΔT [°C]
15.0	2.8	14.2	120	15.2	15	−0.2
19.4	3.7	15.5	414	20	20	0.0
20.6	3.7	16.1	669	20.9	20.9	0.0
21.1	3.9	16.2	545	21.7	21.8	+0.1
21.1	4.2	16.1	471	22	22.1	+0.1
18.5	3.8	15.7	106	19.2	19.3	+0.1
16.4	3	15.2	52	16.8	16.7	−0.1
16	2.9	16	56	16.3	16.2	−0.1
16.3	3.8	15	103	16.7	16.6	−0.1
16	3.2	14.8	80	16.4	16.2	−0.2
15.4	2.3	14.5	32	15.7	15.6	−0.1
15	2.5	14.3	17	15.4	15.2	−0.2

† Thermal resistances (R_{ct} = 1600°C W^{-1} ; R_{i2} = 80°C W^{-1}). Wind speed values (2.3 < V_∞ < 4.2 m s^{-1}). Irregular and low solar radiation values.

Numerical application gives R_{i2} = 80°C W^{-1}.

Validated results show that an analogical model can correct the surface temperature measurement error to bring it back within the range of the initial calibration value. Subsisting temperature differences $T_s - T_v$ are less than ±0.2°C in the great majority of cases; see Tables 3 and 4.

Two examples can be used to illustrate this fact:

(1) For high level solar radiation (E_0 > 700 W m^{-2}) and low wind speed values, the highest temperature difference $T_m - T_v$ recorded is equal, before model correction, to 0.6°C (Table 3). This difference decreases after correction to a value of $T_s - T_v$ equivalent to −0.1°C.

(2) For lower level solar radiation and high wind speed values (V_∞ = 4.2 m s^{-1}), the greatest temperature difference $T_m - T_v$ recorded was equal, before model correction to −0.9°C (Table 3). This temperature difference decreases after correction to a value of $T_s - T_v$ equivalent to +0.1°C.

6. SIMULATION RESULTS

If we consider that our model is correctly validated we can use it as a predictive model to simulate configurations which differ from the experimental configuration. These simulation results can be applied to a plastic semi-transparent material (PMMA) or to a single pane of ordinary glass.

We used this model to correct measurement errors of a single ordinary pane. This model mainly concerns correction results, as there is no known method for incorporating thermocouples inside a semi-transparent material like ordinary glass. The model does not therefore appear in the results set forth in Tables 6 and 7, whether for real surface temperatures T_v or $T_s - T_v$ differences.

These tables show that our model tends to behave as we would expect it to. For high solar radiation values, calculated surface temperatures T_s are lower than measured surface temperatures T_m. Conversely, where wind speed increases, the model gives higher

Table 5.

T_m (°C)	V (m s^{-1})	T_{af} (°C)	E_0 (W m^{-2})	T_s (°C)
23.7	1.1	15.4	729	22.9
24.9	1	16.1	739	24
25.5	1.1	15.7	745	25.5
16.1	1.4	8.6	738	15.5
16.4	1.2	9	759	15.5
17.6	1.1	9.6	775	16.6
18.2	1.6	10	781	17.9
19.8	1.1	10.7	783	19
20.2	1.1	10.8	775	19.5
21.4	1.1	11.1	748	20.9
21.5	0.9	11.1	724	20.8
21	1.2	11.4	702	20.7

† Thermal resistances (R_{ct} = 1600°C W^{-1} ; R_{i2} = 80°C W^{-1}). Low wind speed values (V_∞ < 1.6 m s^{-1}). High solar radiation values (E_0 > 700 W m^{-2})

Table 6.

T_m (°C)	V (m s^{-1})	T_{af} (°C)	E_0 (W m^{-2})	T_s (°C)
15.3	2.8	14.2	120	15.4
18.9	3.7	15.5	414	19.3
19.9	3.7	16.1	669	20
20.1	3.9	16.2	545	20.4
20.2	4.2	16.1	471	20.8
18	3.8	15.7	106	18.5
16.1	3	15.2	52	16.3
15.9	2.9	15	56	16
15.8	3.8	15	103	15.9
15.5	3.2	14.8	80	15.6
15	2.3	14.5	32	15.1
14.7	2.5	14.3	17	14.8

† Thermal resistances (R_{ct} = 1600°C W^{-1} ; R_{i2} = 80°C W^{-1}). Wind speed values (2.3 < V_∞ < 4.2 m s^{-1}). Irregular and low solar radiation values.

calculated surface temperatures T_s than measured values T_m.

We can therefore conclude that our model can be used for other materials than a plastic semi-transparent material (PMMA).

7. CONCLUSIONS

The various results obtained from real site experimentation allowed us to validate a corrective model for a plastic semi-transparent material (PMMA). In the great majority of cases, we can translate directly measured surface temperature values into extrapolated real surface temperature values using an internal temperature field.

Further, the model can be used predictively to correct measured surface temperatures for materials other than plastic semi-transparent materials.

However, the model presents certain weaknesses.

(1) On the one hand, it is only designed to correct the outside surface temperature in a single pane of semi-transparent material and cannot be used to correct the inside surface temperature for the material, as for this purpose we would have to know the radiative heat exchanges inside the enclosure. Unsteady state simulation would therefore be required. Our laboratory is currently working on this problem.

(2) On the other hand, the model is of vital interest when extreme solar radiation and wind speed climatic conditions occur. Indeed, the model is best adapted to conditions where significant differences occur between real surface temperatures and measured surface temperatures.

REFERENCES

1. P. A. Kinzie, *Thermocouple Temperature Measurement*. John Wiley, New York (1973).
2. B. Cassagne, Contribution à la mesure de température de surface par contact, Thèse de doctorat de l'Université de Nantes, France (1985).
3. J. P. Bardon et B. Cassagne, Temperatures de surface. Mesure par contact. In *Technique de l'ingénieur*, Vol. 1, R 2732, pp. 1–21. ISTRA, Strasbourg (1981).
4. Ph. Cerruti, Mesures de températures de surfaces de parois semi-transparentes, Thèse de doctorat de 3^{ieme} cycle de l'Université de Nantes (1986).
5. E. Werling, Contribution aux mesures par contact de températures de surfaces de parois semi-transparentes. Modélisation–expérimentation, Thèse de doctorat de L'Institut National des Sciences Appliquées de Lyon (1988).
6. H. Grenier, Contribution à l'étude du comportement thermique de matériaux semi-transparents (plexiglass PMMA et double vitrage) soumis à un ensoleillement naturel. Modélisation–expérimentation–validation, Thèse de doctorat de l'Institut National des Sciences Appliquées de Toulouse (1987).
7. J. A. Moreau, Mesures par thermocouples de la température superficielle d'un matériau semi-transparent soumis à un environnement naturel. Développement d'un modèle analogique appliqué à la correction de ces mesures, Doctorat de l'Institut National des Sciences appliquées de Toulouse (1991).
8. M. Yovanovitch, H. Cordier et J. Coutanceau, Sur la resistance thermique due à un contact unique, Note CRAS, Paris, T-268-B1 (1969).
9. B. Cassagne, Notion sur la résistance thermique de constriction en régime transitoire, *Journée SFT*, Paris (1986).
10. J. P. Bardon, La mesure des températures de surfaces par contact. Erreurs liées aux transferts de chaleurs parasites, Revue générale de thermique No. 170, pp. 123–135 (1976).
11. A. Degiovanni, G. Sinicki, A. Gery et M. Laurent, Un modèle de resistance thermique de contact en régime permanent, *Revue Gén. Therm.* No. 267, pp. 161–175 (1984).
12. J. P. Bardon, Contribution à l'étude des échanges de chaleur au contact de deux matériaux, Thèse de doctorat d'Etat, Université de Poitiers (1965).
13. *Ashrae Handbook—Fundamentals* (S.I. Edition) (1989).
14. A. Grelat et R. Fauconnier, Rapport de recherche 506/107, CEBTP—Division Thermique, Paris (1980).
15. M. N. Ozisik, *Heat Transfer: A Basic Approach*. Mechanical Engineering Series, McGraw-Hill, New York Company (1985).
16. P. Clergue, Recherche d'une méthode de mesure pour déterminer le coefficient d'émissivité de matériaux non opaques, Rapport de stage IUT de Toulouse, CERT–DERTS (1989).

APPENDIX A. SUPERFICIAL HEAT EXCHANGE COEFFICIENT DETERMINATION

A.1. *Case of radiative exchange coefficients*

We retained linearised values where T_c represents the head sensor temperature and T_b that for the equivalent bar.

Generally speaking, exchanges can be expressed as follows:

$$\Phi_{12} = H_r \times S_1(T1 - T2)$$

where H_r represents the linearised superficial exchange coefficient.

We thus obtain:

$H_{rc} = 4 \times \varepsilon_c \times \sigma \times T_c^3$ for the sensible part of the sensor;

$H_{rb} = 4 \times \varepsilon_c \times \sigma \times T_b^3$ for the equivalent bar.

A.2. *Case of convective exchange coefficients*

A.2.1. *Case of sensor.* As the convective heat exchange could not be determined accurately, we assumed that the flux density φ_{mst} can be divided into two components.

The first components φ_1 concerns the evacuated flux density of the semi-transparent material, and is expressed by the following relation:

$$\varphi_1 = H_{c1} \times (T_s - T_{af}).$$

The second component φ_2 concerns the evacuated flux density for the sensor head and is expressed by the following relation:

$$\varphi_2 = H_{c2} \times (T_{ms} - T_s).$$

For H_{c1} a relation developed in terms of wind speed [13] was retained:

$$H_{c1} = 3.04 \times (V + 0.6)^{0.605}.$$

For H_{c2}, relations taking temperature differences into account were retained, expressed as follows [14]:

$$H_{c2} = 1.88 \times \mathrm{ABS}(T_s - T_{af})^{0.32}.$$

A.2.2. *Case of equivalent bar.* The presence of the equivalent bar for the convective limit flow can be taken into account through the coefficient H_{cb}. This coefficient is expressed by the following relation [15]:

$$H_{cb} = \frac{\lambda}{D_b}(0.4 \times Re_b^{0.5} + 0.06 \times Re_b^{2/3}) \times P_r^{0.66}$$

where Re_b represents the Reynolds number related to the equivalent bar.

B. RADIATIVE CHARACTERISTICS

Certain calculations need knowledge of the short and long wavelength absorption and emissivity coefficients for the sensitive part and the equivalent bar of the sensor.

Values provided in Table B1 are obtained from measurements and detailed calculations [16].

Table B1. Radiative characteristics of different parts of thermocouple

Type of coefficient	Head of sensor	Equivalent bar
Short wavelength absorption coefficient	0.177	0.389
Long wavelength emissivity coefficient	0.95	0.31